Research Article | Vol. 26, No. 18 | 3 Sep 2018 | OPTICS EXPRESS 23132
Optics EXPRESS

Light extraction enhancement and directional control of scintillator by using microlens arrays

XUEYE CHEN,[1] BO LIU,[1,*] JINGTAO ZHU,[1] MU GU,[1] HONG CHEN,[1] JINLIANG LIU,[2] LIANG CHEN,[2] AND XIAOPING OUYANG[2]

[1]*Shanghai Key Laboratory of Special Artificial Microstructure Materials and Technology, School of Physics Science and Engineering, Tongji University, Shanghai 200092, China*
[2]*State Key Laboratory of Intense Pulsed Radiation Simulation and Effect, and Radiation Detection Research Center, Northwest Institute of Nuclear Technology, Xi'an 710024, China*
*lbo@tongji.edu.cn

Abstract: The total internal reflection restricts light extraction efficiency of scintillator, leading to reduced detection efficiency and signal-to-noise ratio in the field of scintillator-based radiation detection system. This research presents the method of applying microlens arrays to improve the light extraction efficiency as well as achieve directional control of emission for scintillators. For BGO ($Bi_4Ge_3O_{12}$) scintillator covered with PMMA (polymethyl-methacrylate) hemispherical microlens array, the 2.59-fold in particular angle (θ_{em} = 45°) and overall 1.94-fold angle-integrated enhancement ratios have been obtained. Furthermore, we analyze and optimize some parameters of microlens arrays such as the packing arrangement, duty ratio, size, refractive index, and shape. As a result, when the refractive index of microlens is slightly larger than that of scintillator, a maximum 6.23-fold angle-integrated enhancements can be achieved. It can be concluded that the microlens array covered on scintillator has considerable value for practical applications on radiation detection.

OCIS codes: (350.3950) Micro-optics; (160.2540) Fluorescent and luminescent materials.

1. Introduction

The application of scintillators that convert the deposited energy after ionizing radiation into scintillation light in the visible or near-visible ranges is of great significance in industrial and scientific research, including nuclear physics experiments, nuclear medical imaging, national security [1,2]. In the field of scintillator-based radiation detection, a high light output is essential for the enhancement of the sensitivity, signal-to-noise ratio as well as energy resolution [3].

The efficient light output for scintillator-based radiation detection systems strongly lies on the luminescence conversion efficiency (internal quantum efficiency) and the light extraction efficiency (external quantum efficiency). Despite the high internal quantum efficiency for most practical scintillators, the total internal reflection (TIR) inside the scintillator lessens the light output. According to Snell's law, scintillation light with an incident angle larger than the critical angle could be trapped inside the scintillator [4]. Consequently, it will leak at the edge of the scintillator or be self-absorbed by the scintillator, limiting light extraction efficiency. For example, according to the approximate formula of ($1/4n^2$) [5], the extraction efficiency of $Bi_4Ge_3O_{12}$ (BGO) scintillator (refractive index n = 2.15 at wavelength of emission peak) with a plane surface is as low as 5.4% from one side of the scintillator-air interface. Besides, the output light usually follows a Lambertian angular profile instead of specific directionality, reducing the light collection efficiency in some scintillator-based radiation devices.

Over the past few years, different kinds of microstructures were widely used to improve the external quantum efficiency of scintillators as well as directional control, such as plasmonic lattice [6,7], photonic crystals fabricated by electron beam lithography [8], soft-X-ray interference lithography [9], hot embossing [10], self-assembly of nanospheres [11,12],

#338259 https://doi.org/10.1364/OE.26.023132
Journal © 2018 Received 9 Jul 2018; revised 9 Aug 2018; accepted 9 Aug 2018; published 23 Aug 2018

Optics EXPRESS

UV nanoimprinting lithography [13,14]. However, light extraction schemes using plasmonic structures or photonic crystal structures have significant wavelength dependence (spectral distortion) due to the essential feature of sub-wavelength or wavelength scales [15].

A microlens refers to a lens with a diameter of 10 to 100 μm, and the regular arrangement of a series of microlenses constitutes a microlens array, which is extensively applied in collimating or focusing [16], illumination [17] and imaging systems [18,19]. The microlens array can be prepared in large area with low cost [20,21]. Compared with photonic crystals, the size of a microlens is much larger than the operating wavelength, which does not result in significant wavelength dependence or spectral distortion. Microlens arrays can be used to achieve light extraction for light emitting diodes (LEDs) [22–24] and organic light emitting diodes (OLEDs) [25–28] by reducing the loss of TIR at interface.

Scintillators face the similar problem of light trapping due to TIR, which could be overcome by microlens arrays. However, compared with LEDs and OLEDs, scintillators have some special features, such as large area, large thickness and wide wavelength range. Furthermore, in contrast to LEDs and OLEDs, directional control of emission is especially important for scintillators, leading to the different requirements for the design of the microlens arrays. In this paper, we put forward the concept to apply microlens arrays into scintillators, in order to achieve an enhancement of light extraction efficiency and control of the directionality of emission. The design and optimization of the structural parameters of microlens arrays, such as the duty ratio, refractive index and shape of an individual microlens, were performed with Monte-carol ray tracing method, providing a theoretical guidance for the application of microlens arrays on scintillators.

2. Methods of structural design and numerical simulation

Figure 1 displays the schematic illustration of scintillator covered with microlens arrays on its surface and the definition of angles in the simulation. The most common packing arrangements of microlens arrays are hexagonal-packed and square-packed structures. The configuration of scintillator covered with hexagonal-packed hemispherical microlens array is sketched in Fig. 1(a). The receiver set in the simulation is able to collect the data of light intensity of any position (defined as M) in the space, and M can be defined by azimuth angle, emission angle and the distance between the receiver and the center of scintillator (r), which is sketched in Fig. 1(b).

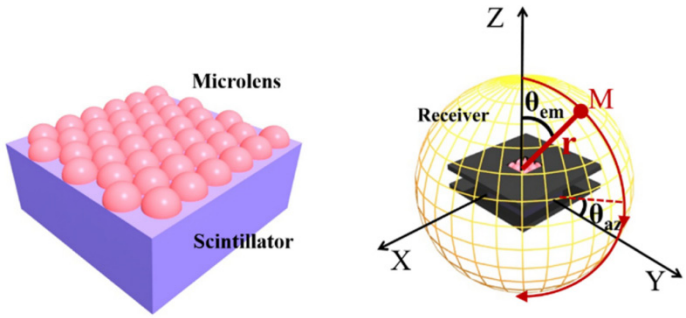

Fig. 1. Schematic illustration of scintillator covered with a hemispherical microlens array (a), the defined coordinate system in simulation (b).

In order to simplify the model in simulation, firstly, we assume that there are two baffles with the size much larger than that of the scintillator fixed to the top and bottom surfaces of scintillator to prevent the stray light and lateral light from entering the receiver. In the center of each baffle, there is one square hole (5 mm × 5 mm) allowing the emission light to propagate both upwards and downwards. Secondly, the receiver is set at infinity in order to

Optics EXPRESS

obtain the far-field intensity. Thirdly, the scintillation light is considered as an isotropic point light source, locating at the center of the scintillator.

The simulation was based on Monte-carol ray tracing method. Light rays were randomly generated, propagating uniformly in all directions. Since there is no wavelength dependence for microlens arrays, the wavelength was selected at 500 nm arbitrarily. The total number of light rays to trace was 1,000,000 and the relative ray power threshold was set to be 1%, suggesting that when the power dropped to be less than 1% of its original energy of the light source, the ray would be terminated.

Figure 2 describes some basic parameters of the microlens arrays, including the duty ratio (D) of the arrays, the size and shape of an individual microlens. As shown in Fig. 2(a), the microlens arrays could be arranged as hexagonal-packed or square-packed structures with the bottom radius (R) and the period (P). D can be defined as the ratio of the area in which microlens arrays contacts the top surface of scintillator to the area of the top surface of scintillator. For a hexagonal-packed microlens array, D can be defined as formula (1).

$$D = \frac{2\pi R^2}{\sqrt{3}P^2} \tag{1}$$

Similarly, for a square-packed microlens array, D can be defined as formula (2).

$$D = \frac{\pi R^2}{P^2} \tag{2}$$

For an individual microlens shown in Fig. 2(b), when the bottom radius is equal to the height (R = H), the microlens is defined as a hemispherical shape. While, when R≠H, the shape is defined by a parabola shape as formula (3), as shown in Fig. 2(c).

$$y=ax^2+b \tag{3}$$

We describe the shape by H/R, H = b, R = $\sqrt{(-b/a)}$, which can be calculated by the parabola formula.

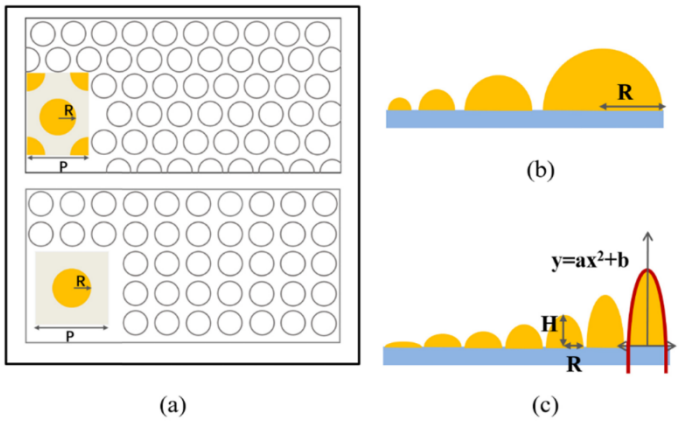

Fig. 2. Schematic illustration of the packing arrangements of hexagonal lattice and square lattice for microlens arrays on the top surface of the scintillator (a), sketch of the scintillator covered with microlens arrays with a hemispherical shape (b) and a parabola shape (c).

3. Results and discussion

In order to verify the feasibility of improving the external quantum efficiency of scintillators by microlens arrays, we take the BGO scintillator covered with polymethylmethacrylate (PMMA) hemispherical microlens array as an example to simulate. The packing arrangement is hexagonal-close-packed. BGO is an extensively used scintillator due to its high light yield

Optics EXPRESS

(8000 photons/MeV), high density (7.13 g/m^3), short radiation length (1.12 cm), as well as great mechanical and chemical durability [29]. BGO plays an important role in gamma-ray medical imaging applications [30] and high-energy physics experiments [31]. Pure PMMA is a thermoplastic polymer which has no light emission under the excitation of high-energy particles and is often applied in the preparation of microlens arrays [32]. Figures 3(a) and 3(b) present the simulated far-field spatial intensity distribution of light emission for the BGO scintillator with plane surface (reference sample) and BGO scintillator covered with a PMMA hemispherical microlens array (bottom radius R = 20 μm) with hexagonal lattice. The size of the BGO scintillator is 5 cm × 5 cm × 1 cm. For the reference sample, the intensity reaches the maximum in the normal direction with an approximate Lambertian angular profile. Nevertheless, for scintillator covered with the hemispherical microlens array, the shape of spatial intensity distribution is of great difference. On the one hand, compared with the reference sample, light extraction efficiency has been greatly enhanced in the whole space. On the other hand, light extraction efficiency reaches the maximum in some particular directions instead of the normal direction. Furthermore, the simulated far-field spatial intensity distribution shown in Fig. 3(b) does not exhibit orientation dependence, which is different from the effect caused by light extraction scheme using photonic crystals [10]. For a more intuitive comparison, Fig. 3(c) presents the results in the two-dimensional polar coordinates. For the scintillator covered with the hemispherical microlens array, the light extraction efficiency reaches the maximum in about θ_{em} = 45°, with an enhancement ratio of 159% compared with the reference sample. While the enhancement ratio in the normal direction is only 28%. This result suggests that significant enhancement of light extraction efficiency in parallel with obvious directional control of light emission can be achieved by a hemispherical microlens array.

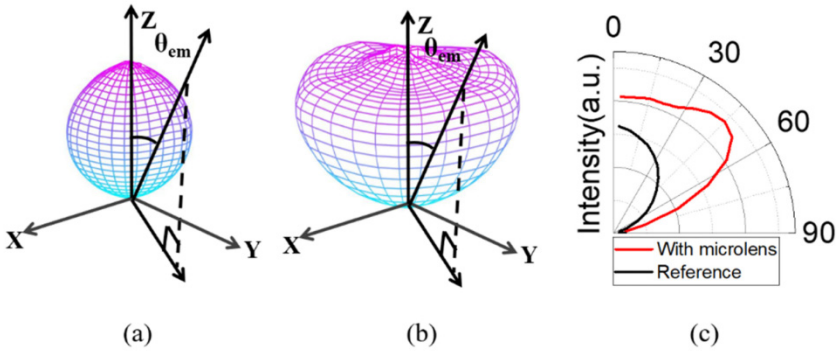

Fig. 3. Simulated spatial distribution of light emission for the reference sample (a) and the sample covered with a PMMA hemispherical microlens array (b), simulated angular profiles of light emission for the reference sample and the sample covered with a PMMA hemispherical microlens array (c).

In order to analyze the mechanism of microlens arrays on light extraction, we have drawn the path of some representative scintillation light beams passing through the plane surface and the surface covered with a hemispherical microlens, shown in Figs. 4(a) and 4(b). According to Snell's law, for a plane surface, the light with incident angle larger than the critical angle θ_1 = arcsin(n_{air}/n_s) will be totally reflected, in which n_{air} is the refractive index of air, and n_s is the refractive index of the scintillator. As a consequence, a large portion of the light will ultimately leak at the edge of the scintillator or be self-absorbed by the scintillator itself instead of escaping from the scintillator and entering the detector. However, when the scintillator is covered with a hemispherical microlens array with refractive index larger than n_{air}, the critical angle will become θ_2 = arcsin(n_{mc}/n_s), in which n_{mc} is the refractive index of the microlens. It is evident that θ_2 is larger than θ_1, indicating that more light beams will have

Optics EXPRESS

chance to get into the hemispherical microlenses and then enter the air through its curved surface.

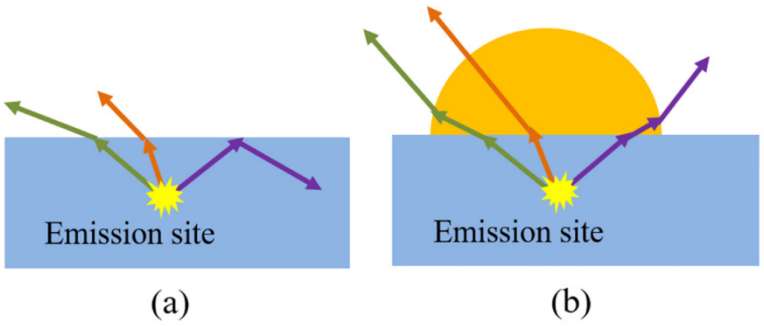

Fig. 4. Path of scintillation light beams passing through the plane surface (a) and the surface covered with a hemispherical microlens (b).

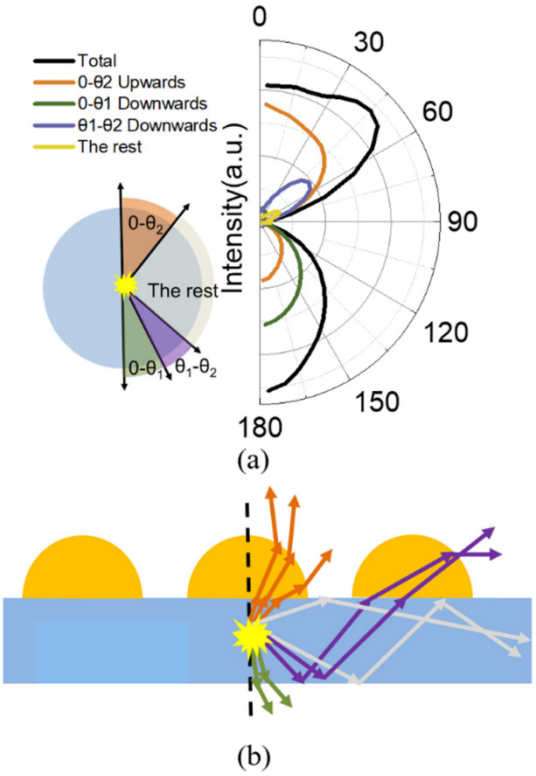

Fig. 5. Simulated angular profiles of emission light divided into different sections (a), path of light from different sections after passing through the surface covered with a hemispherical microlens (b).

To further display the enhancement effect of microlens arrays as well as find out the reasons for directional control, we divide the emission light into several sections, which are namely 0-θ_2 upwards (orange), 0-θ_1 downwards (green), θ_1-θ_2 downwards (purple) and the rest (gray). The simulated angular profiles of light emission are shown in Fig. 5 (a). The overall light extraction efficiency is the superposition of light extraction efficiency of each section. It is found that the section playing a decisive role in directional control is θ_1-θ_2 downwards (purple).

Optics EXPRESS

Figure 5(b) illustrates the path of light from different sections. For upward incident light from 0-θ_2, which is lower than the critical angle of scintillator and the microlens array, the majority of light is extracted through microlens arrays, which is approximately Lambertian and does not contribute to the directional control. Besides, for the plane bottom surface, the downward incident light from 0-θ_1 will escape from the bottom surface, which is of little help to the light extraction efficiency in the upper half space. On the contrary, Light from θ_1-θ_2 downwards can be finally extracted through the microlens after the total reflection on the bottom surface, which is concentrated in a specific angle, leading to significant directionality of emission. In addition, the rest light will be blocked by the baffles or self-absorbed by scintillator.

For the BGO scintillator covered with a PMMA hemispherical microlens array, Fig. 6(a) presents the spatial distribution of light emission when the interfacial property of the bottom surface is set as absorption. Consequently, the downward incident light from θ_1-θ_2 will be absorbed by the bottom surface. The profile of simulated spatial distribution of light emission presented in Fig. 6(a) is approximately Lambertian, which is consistent with the conclusion that the partial reflection on the bottom surface of scintillator contributes to directional control. Figure 6(b) presents the simulated angular profiles of light emission when the interfacial property of the bottom surface is set and not set as absorption.

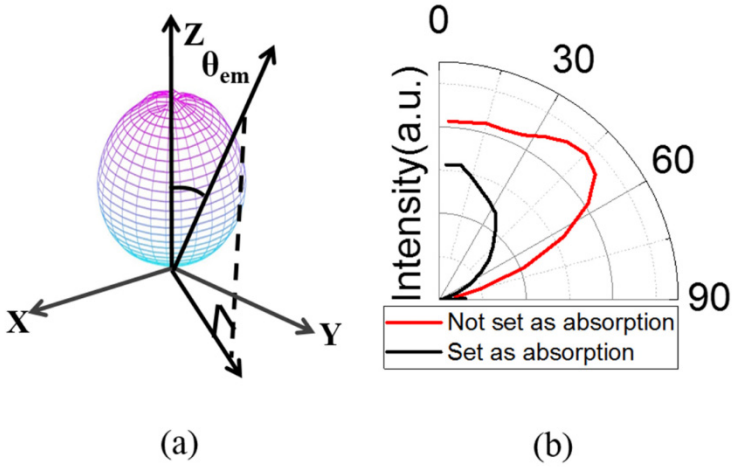

Fig. 6. For the scintillator covered with a PMMA hemispherical microlens array, the simulated spatial distribution of light emission when the interfacial property of the bottom surface is set as absorption (a), simulated angular profiles of light emission when the interfacial property of the bottom surface is set and not set as absorption (b).

Since the size of a microlens is small enough, we assume that the light beams passing through an individual microlens are parallel, shown in Fig. 7(a). According to the spotlight property of a convex lens, the light will converge in θ_{out} when parallel incident light is in θ_{in}. The relationship between θ_{in} and θ_{out} can be described as formula (4).

$$\sin\theta_{in} \cdot n_s = \sin\theta_{out} \cdot n_{mc} \tag{4}$$

According to the effect of Fresnel loss, the smaller the incident angle, the greater the transmittance. As a result, the angle corresponding to the maximum extraction efficiency can be defined as θ_{max}, which can be described as formula (5). The relationship between θ_{max}, n_s, n_{mc} can be described as formulas (6) and (7).

$$\sin\theta_1 \cdot n_s = \sin\theta_{max} \cdot n_{mc} \tag{5}$$

$$\sin\theta_1 \cdot n_s = \sin(\arcsin(1/n_s)) \cdot n_s = 1 \tag{6}$$

Optics EXPRESS

$$\theta_{max} = \arcsin(1/n_{mc}) \quad (7)$$

Formulas (6) and (7) present that θ_{max} depends on n_{mc} instead of n_s. Figure 7(b) presents the simulated angular profiles of emission light from θ_1-θ_2 downwards with the change of n_s when n_{mc} is fixed. Although light extraction efficiency varies, the directionality is consistent. Figure 7(c) presents the simulated angular profiles of emission light from θ_1-θ_2 downwards with the change of n_{mc} when n_s is fixed. Evidently, with the increase of n_{mc}, θ_{max} is getting closer to the normal direction. Simulated angular profiles shown in Figs. 7(b) and (c) meet the expectation in formulas (6) and (7). It should be mentioned that the θ_{max} deduced by formulas (4)-(7) is based on an individual microlens, ignoring the effect of the adjacent microlenses and multiple extraction process due to the TIR on the bottom surface, which can lead to some distinction from the array case.

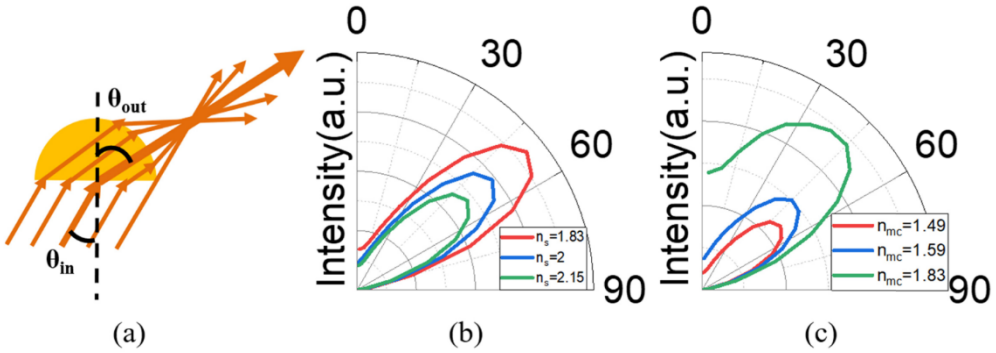

Fig. 7. The schematic diagram of a beam of parallel light passing through a microlens (a), simulated angular profiles of emission light from θ_1-θ_2 downwards with the change of n_s (b) and n_{mc} (c).

Figure 8(a) presents the simulated angular profiles of light emission for the scintillator covered with a hemispherical microlens array with the same duty ratio but different packing arrangements (hexagonal lattice and square lattice). In this simulation, the duty ratio is set to be 22.67%. According to formula (1) and formula (2), for the hexagonal lattice, P/2R = 2, while, for the square lattice, P/2R = 1.86. Figure 8(a) displays the approximately same angular profiles of light emission for microlens arrays with different lattices. Figure 8(b) presents the simulated angular profiles of light emission for the scintillator covered with a hemispherical microlens array with different sizes (R ranging from 10 μm to 100 μm). It is worth mentioning that the duty ratio is fixed (P changes correspondingly with the change of R). The profiles are nearly identical for different R values, indicating that the size and packing arrangement of the microlens arrays do not significantly affect the final light extraction efficiency. Combined with the 360-degree symmetry of simulated spatial distribution of light emission without orientation dependence shown in Fig. 3(b), it suggests that the light extraction enhancement by a microlens array does not depend on the periodic structure, which is completely different from the mechanism of the photonic crystals [12]. The light extraction enhancement by photonic crystals is based on the near-field coupling controlled by dispersion relation. As a result, the light extraction enhancement by photonic crystals is wavelength-dependent, orientation-dependent and may result in spectral distortion. In contrast, the size of a microlens is much larger than the operating wavelength, so that the enhancement mechanism can be explained by geometrical optics, which is not dependent on the wavelength, orientation as well as packing arrangement.

Optics EXPRESS

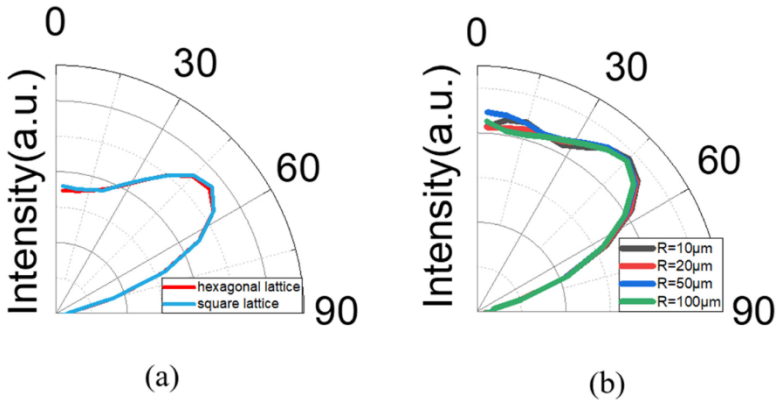

Fig. 8. Simulated angular profiles of light emission for scintillators covered with a hemispherical microlens array with different arrangements but the same duty ratio of 22.67% (a), simulated angular profiles of light emission for the sample covered with a hemispherical microlens array with different sizes but the same duty ratio (b).

Figure 9(a) presents the effect of the duty ratio on light extraction efficiency. For the packing arrangement of hexagonal lattice, the relationship between duty ratio and P/2R is shown in Table 1. The light extraction efficiency increases and then decreases when the duty ratio varies from 90.69% (hexagonal-close-packed) to 3.63%. If the space between adjacent microlenses is too small, the light escaping from one microlens is possible to enter the adjacent microlenses and then return to the scintillator again, thus limiting the light extraction efficiency. While, if the space between adjacent microlenses is too large, even if the light reaches the top surface, it may undergo multiply-TIR process in the scintillator before escaping. This process will increase the possibility of light blocked by the baffles, or self-absorbed by the scintillator itself. Figure 9(b) presents the effect of the refractive index of the microlens on light extraction efficiency. When n_{mc} is equal to 2.5 which is slightly larger than n_s, a maximum 6.23-fold angle-integrated enhancement can be obtained. With the increase of n_{mc}, the critical angle θ_2 between the microlens and the scintillator becomes larger, leading to more light entering the microlenses and getting chance to escape to air through the curved surface of the microlenses. However, when n_{mc} is further increased, the limitation of light extraction caused by TIR inside the microlens will increase, thus reducing the light extraction efficiency. As a result, the refractive index of microlens slightly larger than that of scintillator is preferential. Furthermore, with the increase of n_{mc}, the angle in which intensity reaches the maximum becomes closer to the normal direction, which is consistent with the result in Fig. 7(c). Figure 9(c) reveals the effect of the shape of a microlens (defined by H/R) on light extraction efficiency. When H/R = 0.1, the enhancement is weak and the angular profile is approximately Lambertian, similar to the reference sample. Since light extraction enhancement is mainly realized by the curved surface, the enhancement could be weakened with an oblate microlens array. With the increase of H/R, the angle in which intensity reaches the maximum becomes closer to the normal direction. This implies that the shape of the microlens should be optimized according to the requirement of scintillator-based radiation detection systems.

Table 1. Relationship between duty ratio and P/2R

P/2R	1	1.3	2	5
Duty ratio (D)	90.69%	53.66%	22.67%	3.63%

Optics EXPRESS

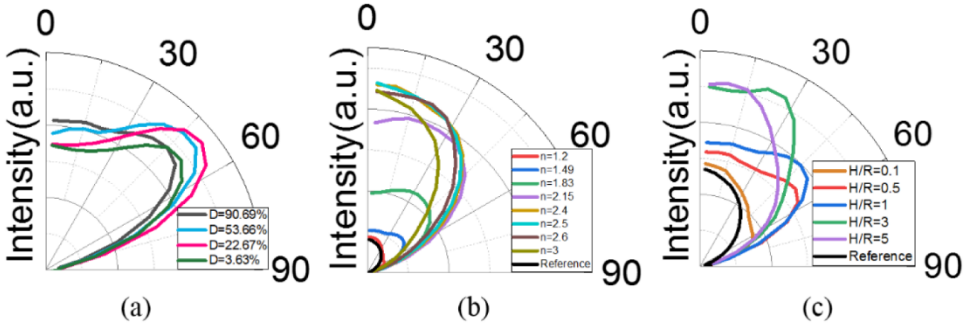

Fig. 9. Simulated angular profiles of light emission for the sample covered with a hemispherical microlens array with different duty ratios (a), different refractive indices (b), different shapes of microlenses (c).

4. Conclusion

In conclusion, we have demonstrated by simulation that a microlens array on the top surface of scintillator is of great value on light extraction efficiency and the directional control of the emission. For BGO scintillator covered with a PMMA hemispherical microlens array, the 2.59-fold in θ_{em} = 45° and overall 1.94-fold angle-integrated enhancement ratios have been obtained. It is found that light extraction enhancement ratio by a microlens array is strongly dependent on the refractive index and shape of the individual microlens. An overall 6.23-fold angle-integrated enhancement can be achieved if the refractive index of microlens is slightly larger than that of scintillator. The enhancement by a microlens array is independent on wavelength, orientation and packing arrangement. In scintillator-based radiation detection systems, the enhancement in a particular direction can be of great benefit to practical applications.

Funding

National Key Research Program of China (Grant No. 2016YFA0301101), the National Natural Science Foundation of China (Grant Nos. 11574230, U1432244), and the Open Project of the State Key Laboratory of Intense Pulsed Radiation Simulation and Effect (Grant No. SKLIPR1516).

References

1. M. Nikl and A. Yoshikawa, "Recent R&D trends in inorganic single-crystal scintillator materials for radiation detection," Adv. Opt. Mater. **3**(4), 463–481 (2015).
2. C. Ronda, H. Wieczorek, V. Khanin, and P. Rodnyi, "Review-scintillators for medical imaging: a tutorial overview," ECS J. Solid State Sci. Technol. **5**(1), R3121–R3125 (2016).
3. F. Tong, B. Liu, H. Chen, Z. C. Zhu, and M. Gu, "Enhanced light extraction of Bi3Ge4O12 scintillator by graded-refractive-index antireflection coatings," Appl. Phys. Lett. **103**(7), 071907 (2013).
4. D. H. Kim, C. O. Cho, Y. G. Roh, H. Jeon, Y. S. Park, J. Cho, J. S. Im, C. Sone, Y. Park, W. J. Choi, and Q. H. Park, "Enhanced light extraction from GaN-based light-emitting diodes with holographically generated two-dimensional photonic crystal patterns," Appl. Phys. Lett. **87**(20), 203508 (2005).
5. B. Kesanli, K. Hong, K. Meyer, H. J. Im, and S. Dai, "Highly efficient solid-state neutron scintillators based on hybrid sol-gel nanocomposite materials," Appl. Phys. Lett. **89**(21), 214104 (2006).
6. B. Liu, Z. Zhu, Q. Wu, C. Cheng, M. Gu, J. Xu, H. Chen, J. Liu, L. Chen, and X. Ouyang, "Plasmonic lattice resonance-enhanced light emission from plastic scintillators by periodical Ag nanoparticle arrays," Appl. Phys. Lett. **110**(18), 181905 (2017).
7. B. Liu, Z. C. Zhu, J. T. Zhu, S. Wu, H. Chen, M. Gu, Q. Cheng, H. Chen, C. W. Cheng, Z. S. Wang, Y. P. Zhao, and Q. L. Zhang, "An approach to achieve significantly faster luminescence decay of thin-film scintillator by surface plasmons," Appl. Phys. Lett. **104**(6), 061902 (2014).
8. A. Knapitsch, E. Auffray, C. W. Fabjan, J. L. Leclercq, X. Letartre, R. Mazurczyk, and P. Lecoq, "Results of photonic crystal enhanced light extraction on heavy inorganic scintillators," IEEE Trans. Nucl. Sci. **59**(5), 2334–2339 (2012).

Optics EXPRESS

9. Z. C. Zhu, S. Wu, C. F. Xue, J. Zhao, L. S. Wang, Y. Q. Wu, B. Liu, C. W. Cheng, M. Gu, H. Chen, and R. Z. Tai, "Enhanced light extraction of scintillator using large-area photonic crystal structures fabricated by soft-X-ray interference lithography," Appl. Phys. Lett. **106**(24), 241901 (2015).
10. X. Chen, B. Liu, Q. Wu, Z. Zhu, J. Zhu, M. Gu, H. Chen, J. Liu, L. Chen, and X. Ouyang, "Enhanced light extraction of plastic scintillator using large-area photonic crystal structures fabricated by hot embossing," Opt. Express **26**(9), 11438–11446 (2018).
11. Z. Zhu, B. Liu, H. Zhang, W. Ren, C. Cheng, S. Wu, M. Gu, and H. Chen, "Improvement of light extraction of LYSO scintillator by using a combination of self-assembly of nanospheres and atomic layer deposition," Opt. Express **23**(6), 7085–7093 (2015).
12. Z. C. Zhu, B. Liu, C. W. Cheng, H. Chen, M. Gu, Y. S. Yi, and R. H. Mao, "Broadband light output enhancement for scintillator using whispering-gallery modes in nanospheres," Phys. Status Solidi., A Appl. Mater. Sci. **211**(7), 1583–1588 (2014).
13. S. Wu, B. Liu, Z. Zhu, C. Cheng, H. Chen, M. Gu, L. Chen, J. Liu, X. Ouyang, C. Xue, and Y. Wu, "Guided-mode resonance assisted directional emission of a wavelength-shifting film for application in scintillation detection," Opt. Express **24**(1), 231–238 (2016).
14. Z. C. Zhu, B. Liu, C. W. Cheng, H. F. Zhang, H. Chen, M. Gu, J. L. Liu, L. Chen, X. P. Ouyang, C. F. Xue, and Y. Q. Wu, "Enhancement of directional broadband luminescence from a scintillation film via guided-mode resonance in a photonic crystal structure," Appl. Phys. Lett. **110**(5), 051901 (2017).
15. A. I. Zhmakin, "Enhancement of light extraction from light emitting diodes," Phys. Rep. **498**(4-5), 189–241 (2011).
16. P. Nussbaum, R. Völkel, H. P. Herzig, M. Eisner, and S. Haselbeck, "Design, fabrication and testing of microlens arrays for sensors and microsystems," Pure Appl. Opt. **6**(6), 617–636 (1997).
17. H. S. Kim, S. I. Moon, D. E. Hwang, K. W. Jeong, C. K. Kim, D. G. Moon, and C. Hong, "Novel fabrication method of microlens arrays with High OLED outcoupling efficiency," Opt. Laser Technol. **77**, 104–110 (2016).
18. Y. M. Song, Y. Xie, V. Malyarchuk, J. Xiao, I. Jung, K. J. Choi, Z. Liu, H. Park, C. Lu, R. H. Kim, R. Li, K. B. Crozier, Y. Huang, and J. A. Rogers, "Digital cameras with designs inspired by the arthropod eye," Nature **497**(7447), 95–99 (2013).
19. T. J. Li, S. Li, Y. Yuan, Y. D. Liu, C. L. Xu, Y. Shuai, and H. P. Tan, "Multi-focused microlens array optimization and light field imaging study based on Monte Carlo method," Opt. Express **25**(7), 8274–8287 (2017).
20. P. H. Huang, T. C. Huang, Y. T. Sun, and S. Y. Yang, "Fabrication of large area resin microlens arrays using gas-assisted ultraviolet embossing," Opt. Express **16**(5), 3041–3048 (2008).
21. J. Yong, F. Chen, Q. Yang, G. Du, H. Bian, D. Zhang, J. Si, F. Yun, and X. Hou, "Rapid fabrication of large-area concave microlens arrays on PDMS by a femtosecond laser," ACS Appl. Mater. Interfaces **5**(19), 9382–9385 (2013).
22. X. H. Lee, I. Moreno, and C. C. Sun, "High-performance LED street lighting using microlens arrays," Opt. Express **21**(9), 10612–10621 (2013).
23. S. I. Chang, J. B. Yoon, H. Kim, J. J. Kim, B. K. Lee, and D. H. Shin, "Microlens array diffuser for a light-emitting diode backlight system," Opt. Lett. **31**(20), 3016–3018 (2006).
24. K. H. Li, C. Feng, and H. W. Choi, "Analysis of micro-lens integrated flip-chip InGaN light-emitting diodes by confocal microscopy," Appl. Phys. Lett. **104**(5), 051107 (2014).
25. Y. H. Ho, K. Y. Chen, K. Y. Peng, M. C. Tsai, W. C. Tian, and P. K. Wei, "Enhanced light out-coupling of organic light-emitting diode using metallic nanomesh electrodes and microlens array," Opt. Express **21**(7), 8535–8543 (2013).
26. W. C. H. Choy, W. K. Chan, and Y. Yuan, "Recent advances in transition metal complexes and light-management engineering in organic optoelectronic devices," Adv. Mater. **26**(31), 5368–5399 (2014).
27. Y. Sun and S. R. Forrest, "Enhanced light out-coupling of organic light-emitting devices using embedded low-index grids," Nat. Photonics **2**(8), 483–487 (2008).
28. S. Möller and S. R. Forrest, "Improved light out-coupling in organic light emitting diodes employing ordered microlens arrays," J. Appl. Phys. **91**(5), 3324–3327 (2002).
29. W. Drozdowski, A. J. Wojtowicz, S. M. Kaczmarek, and M. Berkowski, "Scintillation yield of Bi4Ge3O12 (BGO) pixel crystals," Physica B **405**(6), 1647–1651 (2010).
30. P. Lecoq, "Development of new scintillators for medical applications," Nucl. Instrum. Methods Phys. Res. A **809**, 130–139 (2016).
31. D. Banerjee, V. Burtsev, D. Cooke, P. Crivelli, E. Depero, A. V. Dermenev, S. V. Donskov, F. Dubinin, R. R. Dusaev, S. Emmenegger, A. Fabich, V. N. Frolov, A. Gardikiotis, S. N. Gninenko, M. Hösgen, V. A. Kachanov, A. E. Karneyeu, B. Ketzer, D. V. Kirpichnikov, M. M. Kirsanov, S. G. Kovalenko, V. A. Kramarenko, L. V. Kravchuk, N. V. Krasnikov, S. V. Kuleshov, V. E. Lyubovitskij, V. Lysan, V. A. Matveev, Y. V. Mikhailov, V. V. Myalkovskiy, V. D. Peshekhonov, D. V. Peshekhonov, O. Petuhov, V. A. Polyakov, B. Radics, A. Rubbia, V. D. Samoylenko, V. O. Tikhomirov, D. A. Tlisov, A. N. Toropin, A. Y. Trifonov, B. Vasilishin, G. Vasquez Arenas, P. Ulloa, K. Zhukov, K. Zioutas, "Search for invisible decays of sub-GeV dark photons in missing-energy events at the CERN SPS," Phys. Rev. Lett. **118**(1), 011802 (2017).
32. D. Xie, X. Chang, X. Shu, Y. Wang, H. Ding, and Y. Liu, "Rapid fabrication of thermoplastic polymer refractive microlens array using contactless hot embossing technology," Opt. Express **23**(4), 5154–5166 (2015).